Characterization of circRNAs in established osimertinib-resistant non-small cell lung cancer cell lines

XIN CHEN[1*], JINGYAO GU[1*], JIALI HUANG[2*], KANG WEN[1], GE ZHANG[1], ZHENYAO CHEN[3,4] and ZHAOXIA WANG[1]

[1]Cancer Medical Center, The Second Affiliated Hospital of Nanjing Medical University, Nanjing, Jiangsu 210011; [2]Department of Pharmaceutical Engineering, School of Engineering, China Pharmaceutical University, Nanjing, Jiangsu 210009; [3]Department of Thoracic Surgery, Fudan University Shanghai Cancer Center; [4]Department of Oncology, Shanghai Medical College, Fudan University, Shanghai 200032, P.R. China

Received April 15, 2023; Accepted August 8, 2023

DOI: 10.3892/ijmm.2023.5305

Abstract. Drug resistance is an urgent problem to be solved in the treatment of non-small-cell lung cancer (NSCLC). Osimertinib is a third-generation EGFR-tyrosine kinase inhibitor, which can improve the efficacy and quality of life of patients; however, the inevitable resistance after long-term use of osimertinib often leads to treatment failure. Cell lines are key tools for basic and preclinical studies. At present, few osimertinib-resistant cell lines (HCC827-OR and H1975-OR) have been established. In the present study, osimertinib-resistant cell lines were established by gradually increasing the drug concentration. Half-maximal inhibitory concentration (IC_{50}), cell morphology, whole exon sequencing, Cell Counting Kit-8 assay, EdU staining and flow cytometry were used to evaluate the osimertinib-resistant cell lines. Western blot analysis was used to detect the expression levels of key proteins involved in osimertinib resistance. The circular RNA (circRNA) expression profile was identified by RNA sequencing (RNA-seq) analysis of HCC827, HCC827-OR, H1975 and H1975-OR cells. Subsequently, the biological roles of differentially expressed circRNAs were explored in *in vitro* studies. Osimertinib-resistant cell lines were successfully established via treatment with an increasing concentration of osimertinib. Osimertinib IC_{50} and proliferation of resistant cells were much higher than those of sensitive cells. Notably, phosphorylated (p)-AKT and p-ERK were markedly activated in resistant cells, and the inhibitory effect of osimertinib on p-AKT and p-ERK was weaker in resistant cells than that in parental cells. RNA-seq analysis identified differentially expressed circRNAs in HCC827, HCC827-OR, H1975 and H1975-OR cells. The most dysregulated circRNAs (circPDLIM5 and circPPP4R1) were selected for further functional study. Kyoto Encyclopedia of Genes and Genomes pathway analysis showed that the host genes of differentially expressed circRNAs were associated with 'endocytosis' and 'regulation of autophagy'. In conclusion, the present study established osimertinib-resistant cell lines and revealed that circRNAs may serve as a promising biomarker in NSCLC osimertinib resistance.

Correspondence to: Professor Zhaoxia Wang, Cancer Medical Center, The Second Affiliated Hospital of Nanjing Medical University, 121 Jiangjiayuan Road, Nanjing, Jiangsu 210011, P.R. China
E-mail: zhaoxiawang66@126.com

Dr Zhenyao Chen, Department of Thoracic Surgery, Fudan University Shanghai Cancer Center, 270 Dongan Road, Shanghai 200032, P.R. China
E-mail: czy_556@163.com

[*]Contributed equally

Key words: osimertinib resistance, establishment, circular RNA, non-small cell lung cancer

Introduction

Recent global cancer statistics have shown that the incidence of lung cancer ranks second after breast cancer, and that it has the highest mortality rate among malignant tumors (1). Non-small cell lung cancer (NSCLC) accounts for >80% of all types of lung cancer, and >70% of patients pathologically diagnosed with NSCLC are in the advanced stages, often making them unsuitable for surgery (2). Compared with the stronger toxic side effects of chemotherapy, first-generation EGFR-tyrosine kinase inhibitors (TKIs), such as gefitinib and erlotinib, can significantly improve the efficacy and quality of life of patients with EGFR-sensitive mutations. Resistance is a common problem that affects the efficacy of clinical drugs, and studies on acquired resistance of first-and second-generation EGFR-TKIs have found that the T790M mutation in exon 20 of EGFR is the main mechanism of resistance (3). Based on these results, osimertinib, a third-generation EGFR-TKI was developed, which has been shown to significantly prolong the median progression-free survival and median overall survival (18.9 and 38.6 months, respectively) of patients with advanced NSCLC with an EGFR mutation (4), and has become one of the most effective and safe standard treatment regimens for advanced patients with NSCLC and the EGFR T790M mutation (5). Furthermore, its high blood-brain barrier penetration

can control central nervous system metastasis (6). However, long-term use of osimertinib often results in diminished drug efficacy, rendering patients less sensitive to the drug and leading to treatment failure. Possible mechanisms underlying osimertinib resistance have been reported to include EGFR-dependent and EGFR-independent mechanisms, and also involve alterations in signaling pathways, oncogenic gene fusions and autophagy (7-12); however, the underlying mechanisms remain to be explored. Therefore, constructing osimertinib-resistant NSCLC cell lines *in vitro*, initially exploring the mechanism of osimertinib resistance and identifying methods to reverse drug resistance are important areas in the field of lung cancer research.

Circular RNA (circRNA) is a type of non-coding RNA characterized by a covalently closed loop, which is different from traditional linear RNA. circRNA has the characteristics of tissue specificity and evolutionary conservation, and is not degraded by common exonucleases. It can stably exist in complex intracellular and extracellular environments, and can bind microRNA (miRNA) or protein (13). In addition, circRNA can regulate the expression of downstream genes and is involved in a variety of tumor signaling pathways, where it participates in the regulation of gene transcription, protein translation and other functions, providing a novel direction for NSCLC drug resistance research (14-17). A previous study reported that circFGFR1 serves a role as an oncogene in NSCLC (18). In addition, hsa_circ_0000567 is upregulated in NSCLC cells with acquired gefitinib resistance (19). The expression levels of hsa_circ_0043632 in osimertinib-resistant NSCLC cells are also higher than those in sensitive NSCLC cells; however, the mechanism remains unclear (20).

circRNA serves an important regulatory role in the occurrence and development of lung cancer and drug resistance; however, there are few reports on circRNA and osimertinib resistance in NSCLC (21,22). The present study assessed the abnormal expression of circRNAs in osimertinib-resistant NSCLC and the molecular mechanism underlying the regulation of targeted drug resistance. It will further enrich the current theory of EGFR-TKI resistance and create a new area of study for the investigation of therapeutic methods to overcome EGFR-TKI resistance.

Materials and methods

Cell culture and reagents. NCI-H1975 (EGFR, L858R and T790M mutations) and HCC827 (EGFR, E746-A750 deletion) NSCLC cells were obtained from The Cell Bank of Type Culture Collection of The Chinese Academy of Sciences. Immortalized human umbilical vein endothelial cells (HUVECs) were purchased from Zhongqiao Xinzhou Biotechnology Co., Ltd. (cat. no. ZQY004). H1975 and HCC827 cells were cultured in RPMI 1640 medium (Gibco; Thermo Fisher Scientific, Inc.), whereas HUVECs were cultured in Endothelial Cell Medium (ScienCell Research Laboratories, Inc.). Media were supplemented with 10% fetal bovine serum (Shanghai Yeasen Biotechnology Co., Ltd.), 100 U/ml penicillin and 100 μg/ml streptomycin. All cells were cultured in a humidified incubator at 37˚C with 5% CO_2. Osimertinib, rapamycin (RAPA; cat. no. HY-10219) and 3-methyladenine (3-MA; cat. no. HY-19312) were purchased from MedChemExpress. HCC827, HCC827-OR, H1975 and H1975-OR cells were treated with 10 μM RAPA or 1 nM 3-MA for 24 h at 37˚C, to detect the expression levels of autophagy-related proteins.

Establishment of osimertinib-resistant H1975 and HCC827 cells lines. The osimertinib-resistant H1975 and HCC827 cells were established by continuous exposure to stepwise-increasing concentrations of osimertinib. Osimertinib was dissolved in dimethyl sulfoxide before being added to the cell culture medium. The initial concentrations of osimertinib were equal to the half-maximal inhibitory concentration (IC_{50}) in H1975 (2 nM) and HCC827 (10 nM) cells (23). Cells were then incubated in drug-free medium until the surviving cells had recovered and exhibited a normal exponential growth rate. The dosing was continued at the original concentration until the cells could grow normally at this concentration. Subsequently, the drug concentration was increased until the cells could grow stably. When the drug screening concentration was 5 times the IC_{50} value of parental cells, the concentration difference was increased by 20 nM until the cells could grow stably. When the drug screening concentration was 10 times the IC_{50} value of parental cells, the concentration difference was increased by 50 nM until the cells could grow stably. When the drug screening concentration was 20 times the IC_{50} value of the parental cells, the concentration was increased by 100 nM until the cells could grow stably. After 10 months, the newly established osimertinib-resistant cell lines, which were indicated as H1975-OR and HCC827-OR cells, were maintained in medium containing 1.5 and 2.5 μM osimertinib, respectively. The parental H1975 and HCC827 cells were cultured in drug-free medium in parallel. The drug resistance index (RI) is equal to the IC_{50} value of the resistant cells divided by the IC_{50} value of the parental cells.

Morphological analysis. H1975, H1975-OR, HCC827 and HCC827-OR cells were cultured in a 6-well plate at a density of $1x10^5$ cells/well. After incubation at 37˚C for 24 h, the cellular morphology was observed using an inverted light microscope (Olympus Corporation).

Cell transfection. Plasmids were purified using DNA Midiprep Kits (Qiagen, Inc.) and transfected into cells using Polyjet transfection reagent (SignaGen Laboratories). Small interfering RNAs (siRNAs) against circRNAs and a siRNA negative control obtained from Shanghai Genepharma Co., Ltd. were transfected into cells (HCC827-OR, H1975, H1975-OR) using Lipofectamine® 2000 (Invitrogen; Thermo Fisher Scientific, Inc.) according to the manufacturer's protocol. Cells and siRNAs were incubated with Lipofectamine 2000 at 37˚C for 6 h. Subsequently, the transfection reagents were replaced with complete RPMI 1640 medium. A total of 48 h post-transfection the cells were harvested for subsequent experiments. A total of 100 pmol siRNA was used for transfection in one well of a six-well plate. The siRNA sequences are listed in Table I. circPDLIM5 overexpression plasmid was generated by chemical gene synthesis, and PLVX-puro vector was used as the plasmid backbone (TsingKe Biological Technology). HCC827-OR cells were chosen for plasmid transfection when cell density reached the optimal 70-80%

Table I. Primer and siRNA sequences.

Name	Sequence, 5'-3'
circPLOD2-F	AATGGAAATGGACCCACCAAG
circPLOD2-R	ATCACCACCTCTCCATTCTTCTC
circTNFRSF21-F	GCCATTGTGGAAAAGGCAGG
circTNFRSF21-R	GGCTTGTGTTGGTACAATGCT
circPPP4R1-F	GGGAGTCCGAAAGGCTTGTG
circPPP4R1-R	AGTCATCCACACCAACCAAC
circMUC16-F	GGACCCCATAGTCTCCCCTCT
circMUC16-R	TGCAGGTTGGTGATGGTGAAG
circANKRD11-F	TATACAGCCCTGCTCTGGGA
circANKRD11-R	CTGAAAGTCAGTGCTGACGAG
circGLS-F	AAGGCACAGACATGGTTGGTA
circGLS-R	AACCTTTCCTCCAGACTGCT
circRSF1-F	AAGCTACAGATTCTTCTGTGTGA
circRSF1-R	AGGTGGGCAGAACCATTCTC
circPDLIM5-F	GGAACAACTCAGTCTCGCTCT
circPDLIM5-R	ACACAGCAGGAGATGTAATGGG
circNAV3-F	GACAGTGGCACAAAGCAGTG
circNAV3-R	GGTTGGCCCAGTCAGTGTAA
circSNX13-F	ATGCGATACTTTGTCAGGGAAAT
circSNX13-R	AAGGACAATGCCAAGGCTTCC
GAPDH-F	AGAAGGCTGGGGCTCATTTG
GAPDH-R	AGGGGCCATCCACAGTCTTC
GPC3-F	CCTTTGAAATTGTTGTTCGCCA
GPC3-R	CCTGGGTTCATTAGCTGGGTA
SOX2-F	GCCGAGTGGAAACTTTTGTCG
SOX2-R	GGCAGCGTGTACTTATCCTTCT
AUTS2-F	GGGCTCCGACAAGGAAGAC
AUTS2-R	TGGCGTTTCTCCACACGTTC
CFH-F	GTGAAGTGTTTACCAGTGACAGC
CFH-R	AACCGTACTGCTTGTCCAAAA
SESN3-F	ACCTGCTCTGTACCAACTGC
SESN3-R	GACGACCGGATGTAGAGTATTCT
COL1A2-F	GTTGCTGCTTGCAGTAACCTT
COL1A2-R	AGGGCCAAGTCCAACTCCTT
LOX-F	CGGCGGAGGAAAACTGTCT
LOX-R	TCGGCTGGGTAAGAAATCTGA
VCAN-F	GTAACCCATGCGCTACATAAAGT
VCAN-R	GGCAAAGTAGGCATCGTTGAAA
NNMT-F	ATATTCTGCCTAGACGGTGTGA
NNMT-R	TCAGTGACGACGATCTCCTTAAA
C3-F	GGGGAGTCCCATGTACTCTATC
C3-R	GGAAGTCGTGGACAGTAACAG
ALDH1A1-F	GCACGCCAGACTTACCTGTC
ALDH1A1-R	CCTCCTCAGTTGCAGGATTAAAG
PTPRD-F	CTCCAAGGTTTACACGAACACC
PTPRD-R	AGTCCGTAAGGGTTGTATTCTGA
SPP1-F	CTCCATTGACTCGAACGACTC
SPP1-R	CAGGTCTGCGAAACTTCTTAGAT
SEMA6A-F	AATCAGTATTTCGCATGGCAACT
SEMA6A-R	GCAATGTAGAGGGTTCCGTTCA
UGT3A1-F	AGTCCATCTTCCATCCCCGA
UGT3A1-R	AACAGCCCTGAATGGGCTAC

Table I. Continued.

Name	Sequence, 5'-3'
TMPRSS11E-F	CCTGGCAGTGTGCATTGGA
TMPRSS11E-R	CAAGTCTCTGGCTCATTTCTGT
ALDH1L2-F	GCTGAAGTTGGCACTAATTGGC
ALDH1L2-R	TGAACACCCCTACTACTCGGT
SPTB-F	CCAGCCACCTTACAGCAGG
SPTB-R	TGCGAGTTCACCCATTTCGT
SPARC-F	TGAGGTATCTGTGGGAGCTAATC
SPARC-R	CCTTGCCGTGTTTGCAGTG
NRK-F	AGGGAGGTCACGGATCTGG
NRK-R	CATAAGTACCAAGGCCAATGGTT
si-circPPP4R1-1#-sense	CGUUGGUUGGUGUGGAUGATT
si-circPPP4R1-1#-antisense	UCAUCCACACCAACCAACGTT
si-circPPP4R1-2#-sense	UUGGUUGGUGUGGAUGACUTT
si-circPPP4R1-2#-antisense	AGUCAUCCACACCAACCAATT
si-circPDLIM5-1#-sense	AGAAGGCAAAAGCAUCUGCTT
si-circPDLIM5-1#-antisense	GCAGAUGCUUUUGCCUUCUTT
si-circPDLIM5-2#-sense	AAAGAAGGCAAAAGCAUCUTT
si-circPDLIM5-2#-antisense	AGAUGCUUUUGCCUUCUUUTT
si-NC-F	UUCUCCGAACGUGUCACGUTT
si-NC-R	ACGUGACACGUUCGGAGAATT

circ, circular; F, forward; NC, negative control; R, reverse; siRNA/si, small interfering RNA.

confluence at the time of transfection. A total of 1 μg plasmid was used for transfection in one well of a six-well plate. Cells and plasmids were incubated with Polyjet at room temperature for 15 min. Cells were harvested for subsequent experiments 48 h post-transfection. An empty PLVX-puro vector was used as the negative control for plasmid transfection.

RNA extraction and reverse transcription-quantitative PCR (RT-qPCR) analyses. Total RNA was extracted from H1975, H1975-OR, HCC827 and HCC827-OR cells using TRIzol® reagent (Invitrogen; Thermo Fisher Scientific, Inc.), according to the manufacturer's protocol. RNA was digested with RNase R (Epicentre; Illumina, Inc.) to eliminate linear RNAs and enrich circRNAs. RNA was not digested with RNase R when detecting linear RNAs. Subsequently, total RNA (1.0 μg) was reverse transcribed to cDNA using a Reverse Transcription kit (Takara Biotechnology Co., Ltd.) according to manufacturer's protocol, and qPCR analyses were performed using SYBR Green (Takara Biotechnology Co., Ltd.) to determine the relative expression levels of the specific genes. qPCR was

performed as follows: Initial denaturation at 95˚C for 30 sec; 40 cycles at 95˚C for 5 sec and 60˚C for 34 sec; followed by melting curve at 95˚C for 5 sec and 60˚C for 60 sec. The primer sequences are listed in Table I. Relative mRNA expression levels were analyzed using the $2^{-\Delta\Delta Cq}$ method with GAPDH as the control (24).

Next-generation sequencing. DNA was extracted from the cell samples according to the instructions of the DNA extraction kit (cat. no. DC102-01; Vazyme Biotech Co., Ltd.). DNA quantification was performed on the Qubit 3.0 Fluorometer (Thermo Fisher Scientific, Inc.) with the dsDNA HS Assay kit (Thermo Fisher Scientific, Inc.). The DNA was purified using VAHTS DNA Clean Beads (cat. no. N411-02; Vazyme Biotech Co., Ltd.), and was then fragmented and DNA libraries were constructed using the KAPA Hyper Prep kit (KAPA Biosystems; Roche Diagnostics) according to the manufacturer's instructions. The loading concentration of the final library was 1.75 nM. The concentration was measured by qPCR analysis as aforementioned with the standard curve (25). A panel targeting 139 cancer-related genes (GeneseeqPrime™; Geneseeq Technology, Inc.) using customized xGen lockdown probes (Integrated DNA Technologies, Inc.) was used for hybridization capture. The hybridization reaction was performed with Dynabeads M-279 (Thermo Fisher Scientific, Inc.), and xGen lockdown hybridization and wash kit (Integrated DNA Technologies, Inc.). The target-enriched libraries were sequenced on the Illumina Hiseq4000 NGS platform (HiSeq 3000/4000 SBS kit, cat. no. FC-410-1001; HiSeq 3000/4000 SR Cluster kit, cat. no. GD-410-1001; HiSeq 3000/4000 PE Cluster kit, cat. no. PE-410-1001; HiSeq 4000 Sequencing System, cat. no. SY-401-4001; all from Illumina, Inc.) using the 150 bp paired-end reading according to the manufacturer's protocol. Somatic single nucleotide variants and small insertion/deletions were called by VarScan2 (26). Copy number variation (CNV) was screened using CNVkit (27). A fold-change of >1.50 was considered to be a copy number gain and <0.65 was defined as copy number loss.

High-throughput RNA sequencing (RNA-seq). The preparation of whole transcriptome libraries and deep sequencing was performed by Shanghai BIO Biotech. VAHTS Total RNA-Seq(H/M/R) Library PrepKit for Illumina (cat. no. NR605-02; Vazyme Biotech Co., Ltd.) was used to prepare RNA samples for sequencing. The RNA integrity number of the extracted RNA was assessed using an Agilent Bioanalyzer 2100 (Agilent Technologies, Inc.). Qubit®2.0 Fluorometer (Thermo Fisher Scientific, Inc.) was used to detect the concentration of the library and Agilent 4200 (Agilent Technologies, Inc. was used to detect the size of the library; the loading concentration and volume of the final library was 35 ng/μl and 15 μl. High-throughput RNA-seq was then performed after sequencing reagents were prepared according to the Illumina user guide. Resulting libraries were sequenced initially on an Illumina nova-seq instrument (HiSeq X Ten Reagent kit v2.5, cat. no. FC-501-2501; HiSeq X Ten System, cat. no. SY-412-1001; both from Illumina, Inc.) that generated paired-end reads of 150 nucleotides. Quality control standards for sequencing results were as follows: The amount of data was ~15 G/sample, and Q20 ratio (%) was not less than 90%. Finally, the clean reads were compared with the reference genome using an algorithm for aligning sequence reads against the reference genome (BWA-MEM; https://github.com/lh3/bwa) with default parameters. The reference genome used was GRCh38. For mRNA analyses, the RefSeq (http://www.ncbi.nlm.nih.gov/RefSeq) and Ensemble (https://www.ensembl.org/index.html) transcript databases were chosen as the annotation references. CircRNA distribution in the genome was explored by comparing the circRNA sequence with the genome. The host linear transcripts were annotated according to the location of the circRNA sequence in the chromosome. The expression of circRNAs was calculated using junction reads at the back-splicing sites, and SRPBM was used to normalize the reads. SRPBM value was calculated using the following formula: SRPBM=(SR x10^9)/N, in which SR is the number of spliced reads, and N is the total number of mapped reads in samples. The differential analysis of circRNAs between the two groups (HCC827 vs. HCC827-OR, H1975 vs. H1975-OR) was performed using the negative binomial distribution test based on the DESeq package (https://www.rdocumentation.org/packages/DESeq/versions/1.24.0). Hierarchical clustering analysis between the two groups (HCC827 vs. HCC827-OR, H1975 vs. H1975-OR) was conducted using the R stats package (https://www.rdocumentation.org/packages/stats/versions/3.6.2). After the P-value was obtained via Fisher's exact test, the P-value threshold was determined by false discovery rate. The differential expression multiple (fold-change) was also calculated based on the SRPBM values. There were two criteria used to screen for differentially expressed genes, as follows: One was the fold-change of the same circRNA between two groups, indicating how much the expression value of this gene differs between the two groups, and the other was P-value ($P<0.05$) or false discovery rate, showing whether the results can be trusted.

Functional and pathway enrichment analysis of the host genes of differentially expressed circRNAs. According to the position information of circRNAs, the protein-coding gene corresponding to the genomic position of circRNA can be obtained using CIRI software (https://sourceforge.net/projects/ciri/files/CIRI-full/CIRI_Full_v2.1.1.jar/download), which is known as the host gene. Gene Ontology (GO) and Kyoto Encyclopedia of Genes and Genomes (KEGG) enrichment analyses were performed on the host genes of the differentially expressed circRNAs via the clusterProfiler package. clusterProfiler (https://bioconductor.org/packages/release/bioc/html/clusterProfiler.html) is a Bioconductor-dependent R software package that automates the biological term classification process and gene cluster enrichment analysis.

Sanger sequencing. circPDLIM5 and circPPP4R1 sequences were obtained using divergent primers sent to TsingKe Biological Technology for Sanger sequencing analysis. Primers are listed in Table I.

Calculation of IC_{50}. The IC_{50} values were determined using the Cell Counting Kit 8 (CCK8) cell viability assay (cat. no. 40203ES80; Shanghai Yeasen Biotechnology Co., Ltd.). H1975, H1975-OR, HCC827 and HCC827-OR cells were

seeded ($3.0x10^3$ cells/well) in 96-well plates. Subsequently, 0.25, 0.5, 1, 2, 4, 8, 16 and 32 nM osimertinib were added to H1975 cells; 5, 10, 20, 40, 80, 160, 320 and 640 nM osimertinib were added to HCC827 cells; 0.25, 0.5, 1, 2, 4, 8, 16 and 24 μM osimertinib were added to H1975-OR cells; 0.5, 1, 2, 4, 8, 12, 16 and 32 μM osimertinib were added to HCC827-OR cells. After treatment with osimertinib for 72 h at 37˚C, 100 μl CCK8 solution was added to each well (1:10 dilution) for 2 h at 37˚C, after which, the absorbance was measured at 450 nm. According to drug concentration and corresponding OD value, the drug concentration-cell inhibition rate curve was drawn to calculate IC_{50} values.

Cell proliferation assays. Cells were seeded at a density of $2.0x10^3$ cells/well in 96-well plates. Six replicate wells were used for each analysis. The untransfected cells were cultured in different concentrations of osimertinib (HCC827 and HCC827-OR cells: 0, 15 nM and 6.5 μM osimertinib; H1975 and H1975-OR cells: 0, 2.5 nM and 2.5 μM osimertinib). The transfected cells were cultured in 0 and 1 μM osimertinib. The CCK8 solution was added to each well prior to the endpoint of incubation at a 1:10 (v/v) dilution per 100 μl, and was incubated for 2 h at 37˚C. Cell viability was determined by measuring the absorbance of the converted dye at 450 nm.

EdU assay. The cellular proliferative capability was assessed using the EdU assay kit (Guangzhou RiboBio Co., Ltd.). Cells were cultured in 24-well plates at $2x10^4$ cells/well. Subsequently, 50 μM EdU labeling medium was added to the 24-well plates and they were incubated for 2 h at 37˚C. The following experimental procedures were performed at room temperature. After treatment with 4% paraformaldehyde for 0.5 h and 0.5% Triton X-100 for 1 h, cells were stained with EdU reaction solution for 30 min. DAPI was used to label cell nuclei. EdU-positive cells were observed and imaged under a fluorescence microscope (Olympus Corporation).

Colony formation assay. The untransfected cells were seeded in a 6-well plate at a density of 1,000 cells/well, and cultured in different concentrations of osimertinib (HCC827 and HCC827-OR cells: 0, 15 nM and 6.5 μM osimertinib; H1975 and H1975-OR cells: 0, 2.5 nM and 2.5 μM osimertinib). The transfected cells were cultured in 0 and 1 μM osimertinib. They were incubated in a cell culture incubator until colony formation occurred for 10 days at 37˚C. The colonies were washed with PBS and fixed with 4% polyformaldehyde for 30 min at room temperature. Subsequently, the colonies were stained with 0.1% crystal violet at room temperature for 30 min. Images of the colonies (>50 cells) were captured using digital camera (Panasonic) and calculated by ImageJ software (version 1.5.3; National Institutes of Health).

Transwell assay. Transwell chambers (MilliporeSigma; pore size, 8.0 μm) were used to assess migration. The transfected cells ($5x10^4$) were directly added to the insert membranes. Serum-free medium containing 0 and 1 μM osimertinib was placed into the upper chamber and medium containing 10% FBS was added to the lower chamber. Following incubation for 48 h at 37˚C, the remaining cells on the upper membrane were removed with cotton wool. Invasive cells were fixed with methanol for 30 min at room temperature and stained with 0.1% crystal violet for 30 min at room temperature. Stained cells were counted under a light microscope (Olympus Corporation) and images were captured.

Flow cytometric analysis. The Annexin V-FITC Apoptosis Detection Kit (cat. no. 556547; BD Biosciences) was used to assess apoptosis. Cells were cultured in a 6-well plate at a density of $1x10^5$ cells/well and were treated with different concentrations of osimertinib (HCC827, HCC827-OR: 0, 15 nM and 6.5 μM; H1975, H1975-OR: 0, 2.5 nM and 2.5 μM) or were transfected with 100 pmol siRNA. After 48 h, the cells in each well were collected and dissolved in 1 ml 1X Annexin V Binding Buffer (cat. no. 51-66121E; BD Biosciences). Subsequently, 10 μl Annexin V-FITC (cat. no. 51-65874X; BD Biosciences) was added and mixed for Annexin V-FITC labeling. The cells were incubated at room temperature in the dark for 15 min. A total of 5 min before analysis, 10 μl PI Staining Solution (cat. no. 51-66211E; BD Biosciences) was added for staining at room temperature in the dark for 15 min. The cellular DNA content in the treated cells was quantified using a FACScan flow cytometer (BD Biosciences) and the results were analyzed using FlowJo software v10.6.2 (FlowJo, LLC,).

For cell cycle distribution analysis, $1x10^5$ cells were treated with different concentrations of osimertinib (HCC827, HCC827-OR: 0, 15 nM and 6.5 μM; H1975, H1975-OR: 0, 2.5 nM and 2.5 μM) or transfected with 100 pmol siRNA. After 48 h, the cells were fixed in ice-cold 70% ethanol. The cells were resuspended in 0.5 ml PI/RNase staining solution (cat. no. 550825; BD Biosciences) and incubated at room temperature in the dark for 15 min. Prior to analysis, the samples can be temporarily stored at 4˚C in the dark. Within 1 h, the samples were quantitatively detected using a FACScan flow cytometer. The results were analyzed using FlowJo v10.6.2 software.

Tube formation assay. A Matrigel-based tube formation assay was performed to assess tumor cell vasculogenesis. Briefly, $2x10^4$/well HUVECs were seeded onto 96-well plates coated with 50 μl Matrigel (BD Biosciences) and allowed to polymerize for 10 min at 37˚C. H1975-OR or HCC827-OR cells transfected with siRNAs were centrifuged at room temperature for 5 min at 300 x g. The conditioned medium containing 0 or 1 μM osimertinib was collected from the supernatant and added to the well. After incubation for 4-6 h at 37˚C, the formation of tube structures was observed under an inverted light microscope, and representative images were captured. Total tubule length and number of tubule branches in each well was calculated by ImageJ software (version 1.5.3). All experiments were repeated independently in triplicate.

Western blot analysis. After treatment with different concentrations (0, 10, 100, 1,000 and 10,000 nM) of osimertinib, cells were lysed with RIPA extraction reagent (Beyotime Institute of Biotechnology) supplemented with a protease and phosphatase inhibitor cocktail (MedChemExpress). Protein concentrations were measured using the BCA Protein Assay Kit (Beyotime Institute of Biotechnology). Proteins (20 μg/lane) were separated by SDS-PAGE on 10% gels and were transferred to

0.22-μm polyvinylidene difluoride membranes. Membranes was blocked with 1X TBS-0.1% Tween-20 (TBST) containing 5% BSA (Beyotime Institute of Biotechnology) with constant agitation for 1 h at room temperature. Membranes were then incubated with primary antibodies (1:1,000) against EGFR (cat. no. 4267), phosphorylated (p)-EGFR (cat. no. 3777), AKT (cat. no. 4685), p-AKT (cat. no. 4060), ERK (cat. no. 4695), p-ERK (cat. no. 4370) (all from Cell Signaling Technology, Inc.), P62 (cat. no. 66184-1-Ig), LC3-I/II (cat. no. 14600-1-AP) and GAPDH (cat. no. 60004-1-Ig) (all from Proteintech Group, Inc.) overnight at 4˚C. HRP-conjugated goat anti-rabbit or anti-mouse IgG H&L pre-adsorbed secondary antibodies (1:10,000; cat. nos. SA00001-2 and SA00001-1; Proteintech Group, Inc.) were then used to incubate the membranes for 1 h at room temperature. Subsequently, the membranes were incubated with Super ECL Detection Reagent (cat. no. 36208ES60; Shanghai Yeasen Biotechnology Co., Ltd.) for 1 min and a chemiluminescence imaging system (cat. no. 5200; Tanon Science and Technology Co., Ltd.) was used for visualization of the blots.

Statistical analysis. Statistical analyses were performed using SPSS 20.0 (IBM Corp.) and GraphPad Prism 9 software (Dotmatics). All experiments were performed at least three times and data are presented as the mean ± standard deviation. When the normality of data distribution and equal variance between groups was met, unpaired Student's t-test was applied in two-group comparisons. For multiple comparisons, one-way ANOVA or two-way ANOVA and Bonferroni post hoc test were used, or Kruskal-Wallis test and Dunn post hoc test were used if the normality of data distribution and equal variance between groups was not met. $P<0.05$ was considered to indicate a statistically significant difference.

Results

Establishment and identification of osimertinib-resistant cell lines. Among the NSCLC cell lines, H1975 and HCC827 are sensitive to osimertinib, although they have different mutations; H1975 cells harbor the L858R/T790M double mutation, and HCC827 cells harbor the E746-A750 deletion. These two cell lines with different gene mutation backgrounds were selected to construct osimertinib-resistant cell lines in the present study, with the aim of understanding the mechanism of osimertinib resistance more comprehensively. Osimertinib-resistant cell lines were induced by increasing the drug concentration. Initially, the parental cells HCC827 and H1975 were cultured to a stable state, and were then treated with osimertinib, the proliferation inhibition rate was detected and the IC_{50} value was calculated, which was used as the initial concentration. The initial concentrations of osimertinib used to treat HCC827 and H1975 cells were 10 and 2 nM, respectively. The dosing was continued at the original concentration until the cells could grow normally at this concentration, after which the drug concentration was increased, as aforementioned. Finally, after 10 months, osimertinib-resistant cell lines were successfully established, named HCC827-OR and H1975-OR (Fig. 1A).

CCK8 assays were then performed to detect the cell viability of the four cell lines in response to treatment with different concentrations of osimertinib. The viability of HCC827-OR and H1975-OR cells did not decrease as markedly as that of HCC827 and H1975 cells (Fig. 1B and C). The IC_{50} values of osimertinib for HCC827 and HCC827-OR cells were 15.04 nM and 6.64 μM, and the IC_{50} values of osimertinib for H1975 and H1975-OR cells were 2.34 nM and 2.38 μM respectively (Fig. 1D and E). The drug RI of HCC827-OR and H1975-OR cells was 441.49 and 1,017.09, respectively.

During the 10 months of exposure to osimertinib, the morphology of cells was markedly changed. HCC827 cells appeared closely linked and clumped, with irregular and unclear cell contours, and a few cells had short pseudofoot protrusions. HCC827-OR cells were not closely connected, with obvious cell contours and a mesenchymal phenotype, including a fusiform appearance. In addition, some cells exhibited long pseudopodia. At a high magnification, the cytoplasmic proportion of HCC827-OR cells was increased compared with that of HCC827 cells (Fig. 1F). At low magnification, H1975 cells were loosely arranged with irregular contours. H1975-OR cells were closely arranged in a spindle shape and grew in clumps. At high magnification, compared with H1975 cells, some H1975-OR cells exhibited pseudopodia and presented a dendritic shape (Fig. 1G).

The present study also performed next-generation sequencing to evaluate the gene mutation status of osimertinib-resistant and -sensitive cell lines. The mutant abundance of T790M was much higher in H1975-OR cells than in H1975 cells. Copy number amplification of AKT1, CDK6 and MYC was also detected in H1975-OR cells (Table SI). The abundance of EGFR and CDK4 mutations were lower in HCC827-OR cells than in HCC827 cells (Table SII). NGS results not only demonstrated the presence of EGFR mutations in the osimertinib-resistant cells constructed for the present study, but also revealed potential drug resistance mechanisms, such as copy number amplification of CDK6, MYC and AKT1, and CDK4 gene mutation. In summary, osimertinib-resistant cell lines were successfully established and the details of these resistant cell lines were identified.

Characterization of the proliferation and drug resistance of osimertinib-resistant and -sensitive cells. After long-term treatment with osimertinib, the cell viability of sensitive and resistant cells was affected. Cell viability was detected by CCK8 assay, and cell proliferation ability and proliferation rate could also be detected. Drug-resistant cells and parental cells were monitored using CCK8 reagent for 5 consecutive days (days 0, 1, 2, 3 and 4). The viability of HCC827-OR cells was higher than that of HCC827 cells on day 1, whereas the difference between the two cell lines on days 2, 3 and 4 was more significant (Fig. 2A). Notably, there was no significant difference in viability between the H1975 and H1975-OR cells (Fig. 2D). Colony formation assays showed that HCC827-OR cells exhibited stronger proliferative ability than HCC827 cells (Fig. 2B), whereas there was no significant difference between H1975-OR and H1975 cells regarding proliferative ability (Fig. 2E). The EdU assay was also used to evaluate the proliferation of these four cell lines, and the results were consistent with those of CCK8 and colony formation assays (Fig. 2C and F).

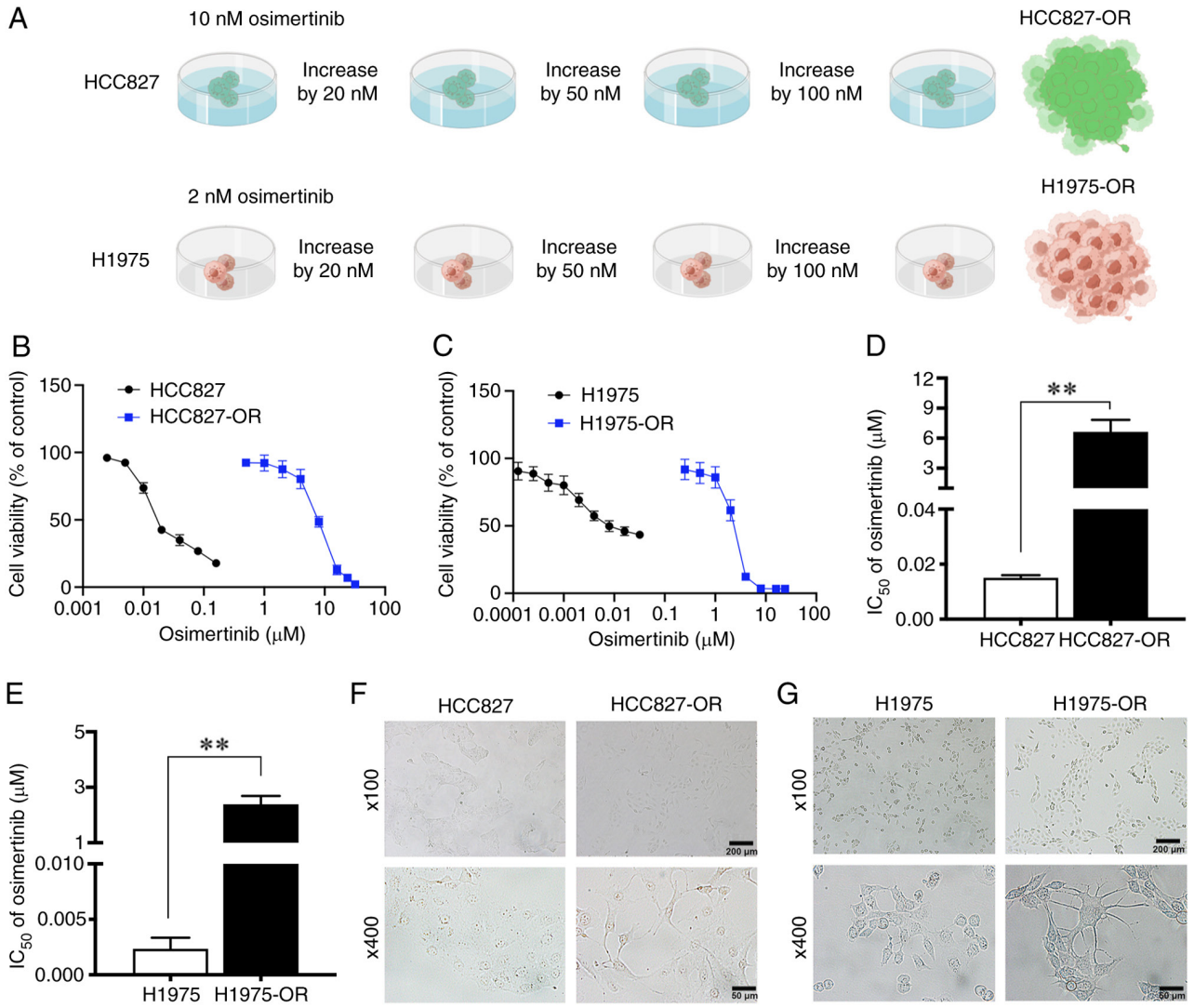

Figure 1. Generation of osimertinib-resistant H1975 and HCC827 cells, H1975-OR and HCC827-OR. (A) Schematic outline of osimertinib-resistant cell line establishment, edited by Figdraw (https://www.figdraw.com/). The drug sensitivity of (B) HCC827 and HCC827-OR cells, and (C) H1975 and H1975-OR cells was detected by CCK8 assay. IC_{50} values of osimertinib in (D) HCC827 and HCC827-OR cells, and (E) H1975 and H1975-OR cells were examined by CCK8 assay. The morphological differences between (F) HCC827 and HCC827-OR cells, and (G) H1975 and H1975-OR cells were observed under a light microscope. $^{**}P<0.01$. CCK8, Cell Counting Kit 8; IC_{50}, half-maximal inhibitory concentration.

To further compare the effects of osimertinib on proliferation of drug-resistant cell lines and parental cell lines, the cells were treated with different concentrations of osimertinib. For HCC827 and HCC827-OR cells, the three treatment groups were 0, 15 nM osimertinib (low concentration) and 6.5 μM osimertinib (high concentration) (Fig. 3A and B). H1975 and H1975-OR cells were treated with 0, 2.5 nM osimertinib (low concentration) and 2.5 μM osimertinib (high concentration) (Fig. 3D and E). The low concentrations of osimertinib significantly inhibited HCC827 and H1975 cell viability, but did not inhibit HCC827-OR and H1975-OR cell viability. The high concentrations of osimertinib significantly inhibited all of the four cell lines. Notably, colony formation of HCC827-OR cells was stronger than that of HCC827 cells, but there was no significant difference between H1975-OR and H1975 cells (Fig. 3C and F). Both low and high concentrations of osimertinib inhibited the colony formation of the parental cells, HCC827 and H1975. The low concentrations of osimertinib did not inhibit the colony formation of drug-resistant cells; however, the high concentrations of osimertinib significantly inhibited the colony formation of HCC827-OR and H1975-OR cells. These results confirmed the effects of osimertinib on the proliferation and drug resistance of osimertinib-resistant and -sensitive cells.

Osimertinib-resistant cells display decreased sensitivity to osimertinib-induced apoptosis and cell cycle arrest. Flow cytometry was used to examine cell cycle distribution and apoptosis in an effort to better understand how osimertinib affects resistant and sensitive cells. Osimertinib was applied to sensitive and resistant cells at various concentrations, as aforementioned. Compared with that in the control group, following treatment with low and high concentrations of osimertinib, the number of HCC827 cells was increased in G_1 phase and decreased in S phase (Figs. 3G and S1A). Compared with that in the control group, following treatment with the high concentration of osimertinib, the number of HCC827-OR cells was increased in G_1 phase and decreased in S phase.

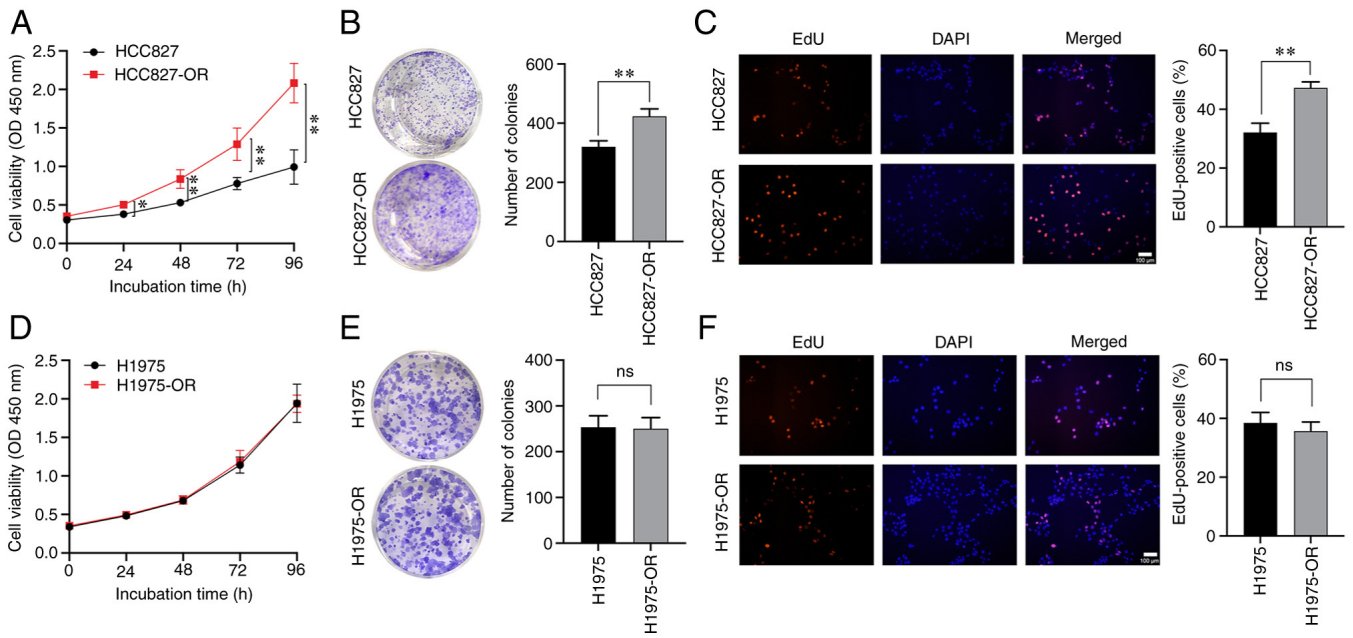

Figure 2. Characterization of the proliferation of osimertinib-resistant and -sensitive cells. HCC827 and HCC827-OR cell proliferation was detected by (A) CCK8 assay, (B) colony formation assay and (C) EdU assay. H1975 and H1975-OR cell proliferation was detected by (D) CCK8 assay, (E) colony formation assay and (F) EdU assay. *P<0.05 and **P<0.01. CCK8, Cell Counting Kit 8; ns, not significant.

Compared with that in the control group, following treatment with low and high concentrations of osimertinib, the number of H1975 cells was increased in G_1 phase and decreased in S phase (Figs. 3H and S1B). Compared with that in the control group, following treatment with the high concentration of osimertinib, the number of H1975-OR cells was increased in G_1 phase and decreased in S phase. These findings indicated that the low concentration of osimertinib exerted considerable influence on the cell cycle distribution of HCC827 and H1975 cells, whereas it had no significant effect on HCC827-OR and H1975-OR cells. However, high-concentration osimertinib could affect the cell cycle distribution of osimertinib-resistant cells and parental cells.

In addition to cell cycle analysis, the effect of osimertinib on the apoptosis of resistant cells and sensitive cells was examined. The low concentration of osimertinib had no significant effects on cell apoptosis in both sensitive and resistant cells. Similar results were observed in H1975 and H1975-OR cells (Fig. 4A and B). By contrast, the high concentration of osimertinib significantly promoted the apoptosis of parental cells. In resistant cells, the high concentration of osimertinib promoted the apoptosis of HCC827-OR cells, but had no significant effect on the apoptosis of H1975-OR cells. Collectively, parental cells appeared to be more sensitive to osimertinib-induced apoptosis and cell cycle arrest.

Characterization of EGFR and downstream proteins in osimertinib-sensitive and -resistant cells. During the development of osimertinib resistance, the levels of some key proteins are changed, including AKT, ERK and EGFR (28). Compared with those in HCC827 cells, the expression levels of EGFR in HCC827-OR cells were decreased, whereas the expression levels of AKT and ERK were not affected. Notably, the expression levels of p-proteins, such as p-EGFR, p-ERK and p-AKT, in HCC827-OR and HCC827 cells were associated with the concentration of osimertinib. The expression levels of p-EGFR, p-ERK and p-AKT in HCC827-OR and HCC827 cells were decreased with the increasing osimertinib concentration (Fig. 4C). The expression levels of p-EGFR in HCC827-OR cells were lower than those in HCC827 cells either in the control group or osimertinib treatment groups. By contrast, the expression levels of p-AKT and p-ERK were higher in HCC827-OR cells than those in HCC827 cells in the same concentration group. In addition, the inhibitory effect of osimertinib treatment on p-AKT and p-ERK was weaker than that of p-EGFR.

After 4 h of osimertinib treatment, the expression levels of p-EGFR, p-AKT and p-ERK were significantly downregulated in H1975 cells (Fig. 4D). Similarly, the expression levels of p-AKT and p-ERK in H1975-OR cells were decreased with the increase in osimertinib concentration. In contrast to H1975 cells, p-EGFR expression in H1975-OR cells was not affected by osimertinib.

Taken together, the expression of EGFR in HCC827-OR and H1975-OR cells was decreased, whereas the expression of AKT and ERK was not markedly affected. In addition, p-AKT and p-ERK of HCC827-OR and H1975-OR were markedly activated compared with those in HCC827 and H1975 cells, and the inhibitory effect of osimertinib on p-AKT and p-ERK was weaker in resistant cells than that in parental cells. Furthermore, the expression levels of p-EGFR were inhibited in HCC827-OR cells, whereas they were not affected in H1975-OR cells treated with various osimertinib concentrations.

These results indicated that the AKT and ERK signaling pathways may be involved in osimertinib resistance, and that the activation of p-AKT and p-ERK may serve an important role in the development of osimertinib resistance.

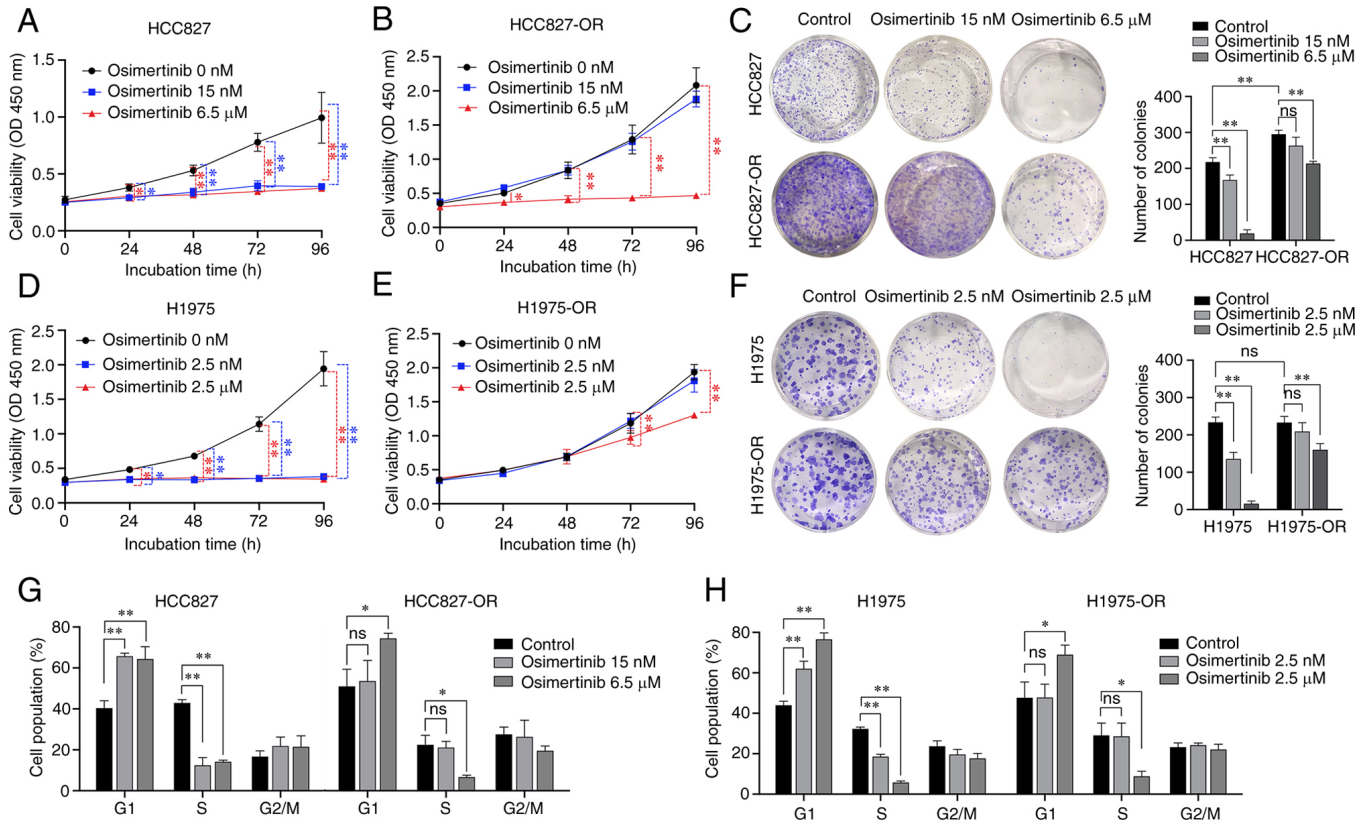

Figure 3. Characterization of sensitivity to osimertinib in osimertinib-resistant and -sensitive cells. (A) HCC827 and (B) HCC827-OR cells were treated with various concentrations of osimertinib, and cell viability was evaluated using CCK8 assay. (C) HCC827 and HCC827-OR cells were incubated with various concentrations of osimertinib for 12 days. Cell colonies were stained with crystal violet and images were captured. (D) H1975 and (E) H1975-OR cells were treated with various concentrations of osimertinib, and cell viability was evaluated using CCK8 assay. (F) H1975 and H1975-OR cells were incubated with various concentrations of osimertinib for 10 days. (G) HCC827 and HCC827-OR cells, and (H) H1975 and H1975-OR cells were treated with various concentrations of osimertinib for 24 h, and cell cycle progression was analyzed by flow cytometry. *P<0.05 and **P<0.01. CCK8, Cell Counting Kit 8; ns, not significant.

circRNA expression profiles and pathway analysis in osimertinib-sensitive and -resistant cells. To identify the differentially expressed circRNAs in osimertinib-resistant cell lines and sensitive cell lines, unbiased RNA-seq analysis of HCC827, HCC827-OR, H1975 and H1975-OR cells was performed. The results of hierarchical clustering suggested that the circRNA expression patterns were distinguishable between resistant and sensitive cells (Fig. 5A and B). A total of 67 upregulated and 142 downregulated circRNAs were identified. Notably, 65 circRNAs were considered new circRNAs with no annotations. GO and KEGG pathway analyses were performed with circRNA host genes to evaluate the roles of differentially expressed circRNAs. The results of KEGG pathway analysis are shown in Fig. 5C and D, while the results of GO analysis are not shown. The host genes of differentially expressed circRNAs in H1975-OR and H1975 cells were mainly associated with 'regulation of autophagy'. Notably, the host genes of differentially expressed circRNAs in HCC827-OR and HCC827 cells were associated with 'endocytosis'. Autophagy can affect endocytosis and cell signaling, and endocytosis can also regulate the different steps of autophagy (29-31). Autophagy and endocytosis serve an important role in drug resistance of NSCLC. The present study subsequently performed western blot analysis to detect the expression levels of autophagy-related proteins in osimertinib-sensitive and -resistant cell lines. Cells were treated with the autophagy agonist RAPA and the autophagy inhibitor 3-MA. Western blot analysis showed that RAPA enhanced the expression levels of autophagy-related proteins, whereas 3-MA inhibited the expression levels of autophagy-related proteins (Fig. 5E and F). Compared with in the parental cells, HCC827-OR and H1975-OR cells exhibited reduced protein expression levels of P62 and an increase in LC3-II conversion, indicating that autophagy was activated in osimertinib-resistant cells and autophagy may be one of the underlying mechanisms of osimertinib resistance.

Validation of the expression level and biological role of circPDLIM5 and circPPP4R1 in osimertinib-resistant and -sensitive cells. The top 10 dysregulated circRNAs are summarized in Tables II and III. RT-qPCR was used to validate the RNA-seq data. The expression levels of those dysregulated circRNAs and mRNAs (including ALDH1A1, PTPRD, TMPRSS11E and SPTB) were measured in HCC827 and HCC827-OR cells (Figs. 6A, and S2A and B). The most dysregulated circRNA (circPDLIM5) was selected for further study. Sanger sequencing was used to confirm the back-splice junction sites of circPDLIM5 (Fig. 6B). To explore the biological role of circPDLIM5 in osimertinib-resistant cells, specific siRNAs targeting the back-splice junction sites of circPDLIM5 were designed and synthesized to silence circPDLIM5 expression (Fig. 6C). si-circPDLIM5 1# was chosen for subsequent experiments

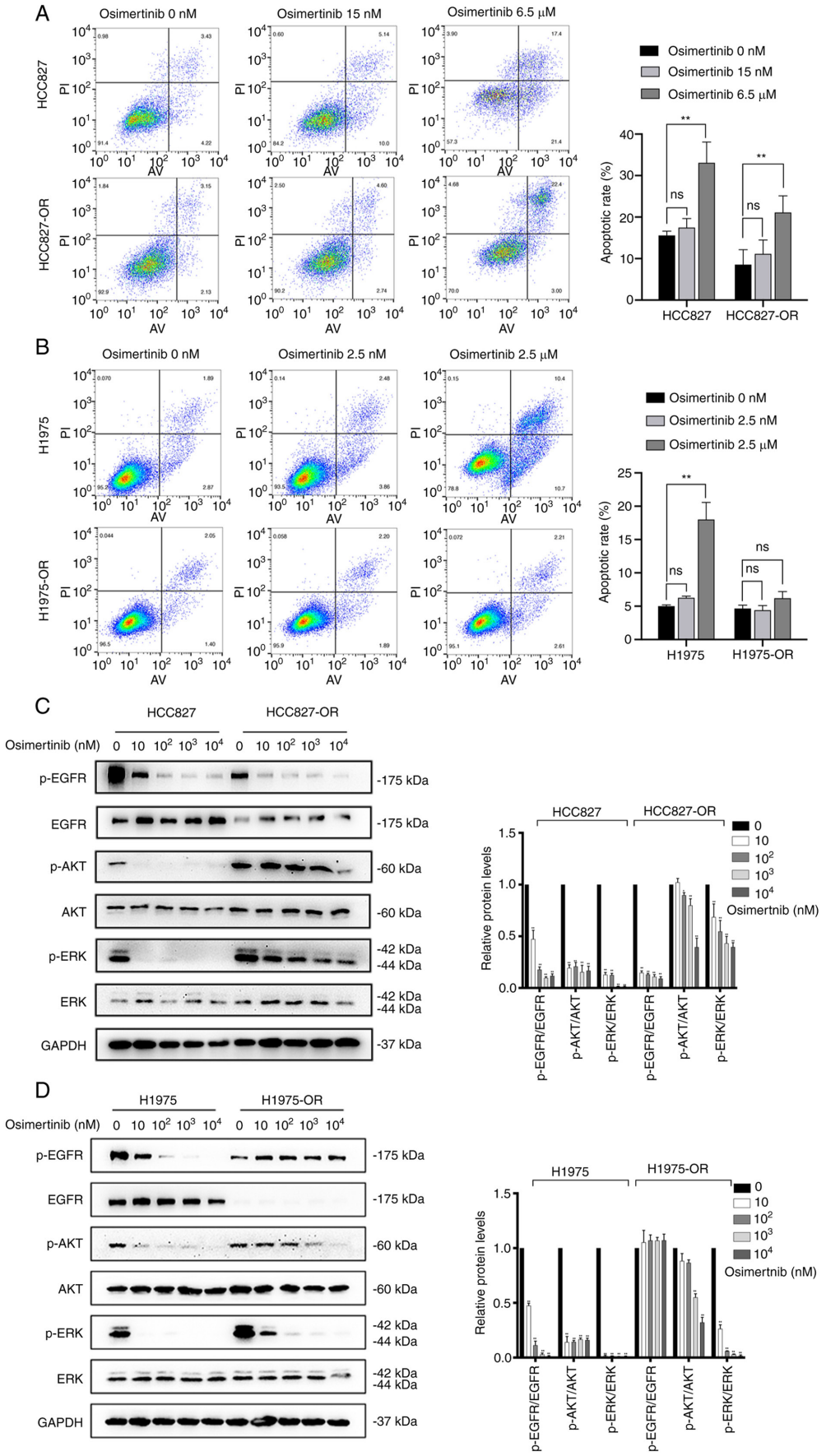

Figure 4. Flow cytometric analysis of apoptosis and detection of key proteins in osimertinib-resistant and -sensitive cells. (A) HCC827 and HCC827-OR cells, and (B) H1975 and H1975-OR cells were treated with various concentrations of osimertinib for 24 h, and the apoptotic cells were stained with annexin V/PI and analyzed by flow cytometry. After treatment with different concentrations of osimertinib for 4 h, western blot analysis was used to determine the changes in the expression levels of key proteins involved in pathway of osimertinib resistance in (C) HCC827 and HCC827-OR cells, and (D) H1975 and H1975-OR cells. Protein levels were semi-quantified. $^{*}P<0.05$ and $^{**}P<0.01$. ns, not significant; p-, phosphorylated.

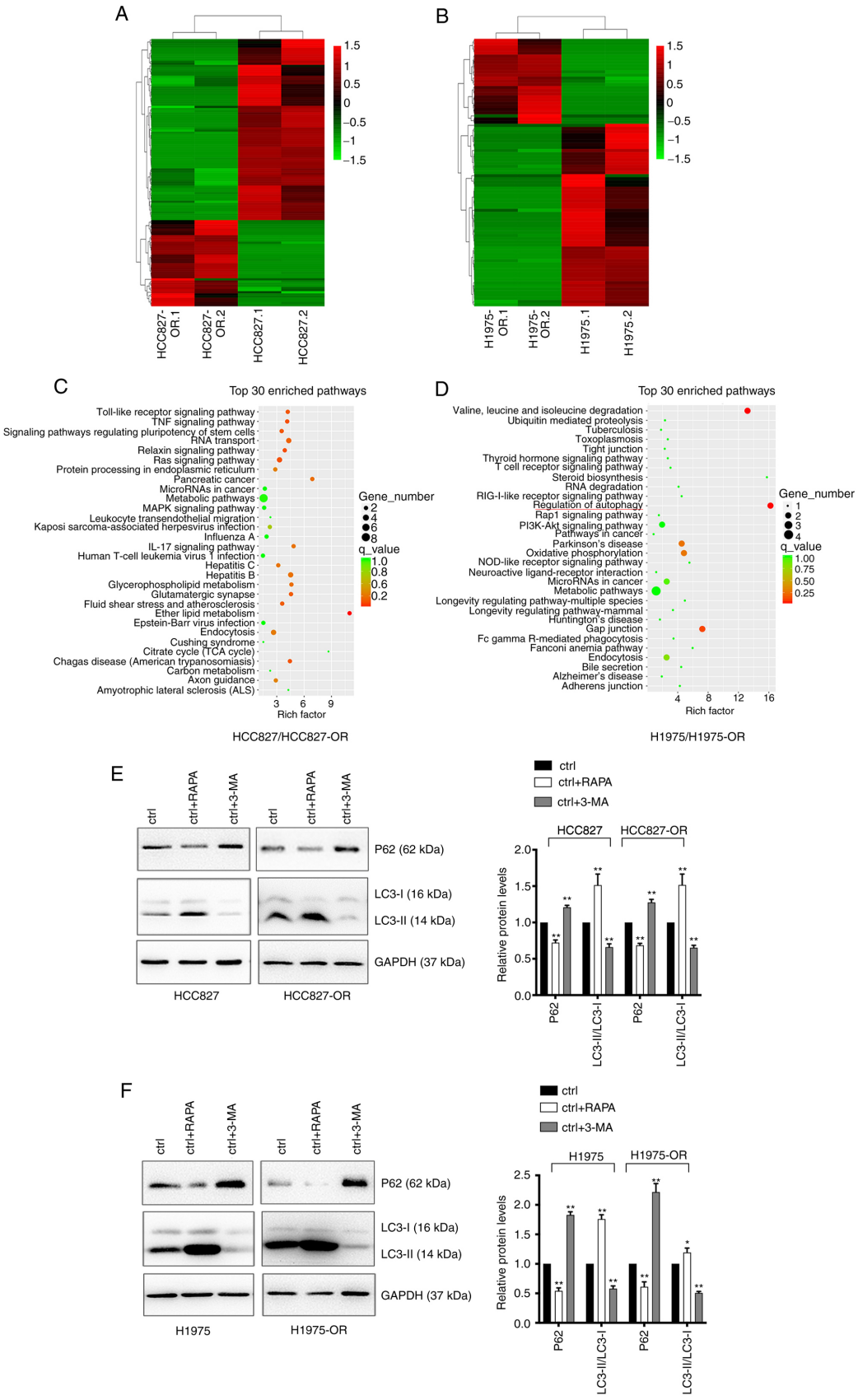

Figure 5. Profiles of differentially expressed circRNAs in HCC827, HCC827-OR, H1975 and H1975-OR cells. Unsupervised hierarchical clustering analysis of the differentially expressed circRNAs between (A) HCC827 and HCC827-OR cells, and (B) H1975 and H1975-OR cells. Kyoto Encyclopedia of Genes and Genomes analysis for the host genes of differentially expressed circRNAs in (C) HCC827 and HCC827-OR cells, and (D) H1975 and H1975-OR cells. Rich factor represents the enrichment degree of differentially expressed genes. The y-axis shows the name of the enriched pathways. The area of each node represents the number of enriched host genes of differentially expressed circRNAs. The P-value is represented by a color scale. (E) HCC827 and HCC827-OR cells, and (F) H1975 and H1975-OR cells were treated with 10 μM RAPA or 1 nM 3-MA for 24 h at 37°C, and the expression levels of autophagy-related proteins were detected by western blot analysis. Western blots were semi-quantified. *P<0.05 and **P<0.01 vs. ctrl. 3-MA, 3-methyladenine; circRNA, circular RNA; ctrl, control; RAPA, rapamycin.

Table II. Top 10 upregulated and downregulated circular RNAs in HCC827-OR cells compared with in HCC827 cells.

circRNA ID	circBase_ID	Chromosome	Gene symbol	log2FC	P-value	Regulation
circANKRD11	hsa_circ_0004566	16	ANKRD11	2.277435	0.001953	Up
circMUC16	-	19	MUC16	1.534303	0.037548	Up
circRYK	hsa_circ_0003633	3	RYK	1.089538	0.026517	Up
circNAV3	hsa_circ_0005450	12	NAV3	1.402228	0.046951	Up
circMKLN1	hsa_circ_0001746	7	MKLN1	1.401088	0.008609	Up
circRSF1	hsa_circ_0000344	11	RSF1	-2.83892	0.039224	Down
circPDLIM5	hsa_circ_0070467	4	PDLIM5	-2.72013	0.00267	Down
circGLS	hsa_circ_0001085	2	GLS	-2.69737	0.000753	Down
circMIB1	hsa_circ_0000836	18	MIB1	-2.51699	0.025407	Down
circOMA1	hsa_circ_0000072	1	OMA1	-2.47581	0.02635	Down

FC, fold change.

Table III. Top 10 upregulated and downregulated circular RNAs in H1975-OR cells compared with in H1975 cells.

circRNA ID	circBase_ID	Chromosome	Gene symbol	log2FC	P-value	Regulation
circSNX13	hsa_circ_0004671	7	SNX13	-3.81645	0.023204	Down
circPLOD2	hsa_circ_0067682	3	PLOD2	-2.98033	0.018598	Down
circTNFRSF21	hsa_circ_0001610	6	TNFRSF21	-2.86512	0.013664	Down
circDCBLD2	hsa_circ_0066631	3	DCBLD2	-2.66131	0.014213	Down
circMPP6	hsa_circ_0001686	7	MPP6	-2.22047	0.020604	Down
circSATB2	hsa_circ_0003915	2	SATB2	-3.71277	0.026945	Down
circMUC16	-	19	MUC16	3.958709	0.00559	Up
circPPP4R1	hsa_circ_0007509	18	PPP4R1	3.193046	0.043673	Up
circSPAG16	hsa_circ_0058040	2	SPAG16	1.857802	0.028686	Up
circMYH9	-	22	MYH9	1.454296	0.015441	Up

FC, fold change.

due to its high interference efficiency. Cell proliferation was measured by the CCK8 assay, and silencing of circPDLIM5 significantly promoted cell proliferation in HCC827-OR cells (Fig. 6D). The colony formation assay showed that knockdown of circPDLIM5 significantly increased the colony-forming ability of HCC827-OR cells (Fig. 6E). In cell cycle and apoptosis analyses, knockdown of circPDLIM5 markedly reduced the apoptotic rate and G_0/G_1 distribution in HCC827-OR cells (Fig. S3A and B). Epithelial-mesenchymal transition and angiogenesis are closely related to the development of osimertinib resistance (32,33); therefore, Transwell migration and angiogenesis assays were performed. Silencing of circPDLIM5 promoted the migration and angiogenesis of HCC827-OR cells (Fig. 6F and G). In addition, circPDLIM5 was overexpressed in HCC827-OR cells; overexpression of circPDLIM5 inhibited cell proliferation and migration, and promoted cell apoptosis (Fig. S3C-G). These findings indicated that inhibition of circPDLIM5 significantly promoted the proliferation, migration and angiogenesis of HCC827-OR cells.

The expression levels of dysregulated circRNAs and mRNAs were also measured in H1975 and H1975-OR cells (Figs. 7A, and S2C and D). circPPP4R1 was chosen as the most dysregulated circRNA in H1975 and H1975-OR cells. Sanger sequencing was used to confirm the back-splice junction sites of circPPP4R1, confirming the head-to-tail splicing in the RT-qPCR product of circPPP4R1 (Fig. 7B). Specific siRNAs targeting the back-splice junction sites of circPPP4R1 were designed and synthesized to silence circPPP4R1 expression (Fig. 7C). si-circPPP4R1 2# was chosen for subsequent experiments due to its high interference efficiency. CCK8 and colony formation assay showed that silencing of circPPP4R1 significantly inhibited cell proliferation in H1975-OR cells (Fig. 7D and E). Knockdown of circPPP4R1 also markedly increased the apoptotic rate and G_0/G_1 distribution in H1975-OR cells (Fig. S4A and B). Inhibition of circPPP4R1 also significantly reduced the migration and angiogenesis of H1975-OR cells, and the inhibitory impact was more pronounced following osimertinib treatment, whereas it had no significant effect on parental H1975 cells (Figs. 7F and G and S4C-G). These results suggested that dysregulated circRNAs may have an important role in NSCLC drug resistance.

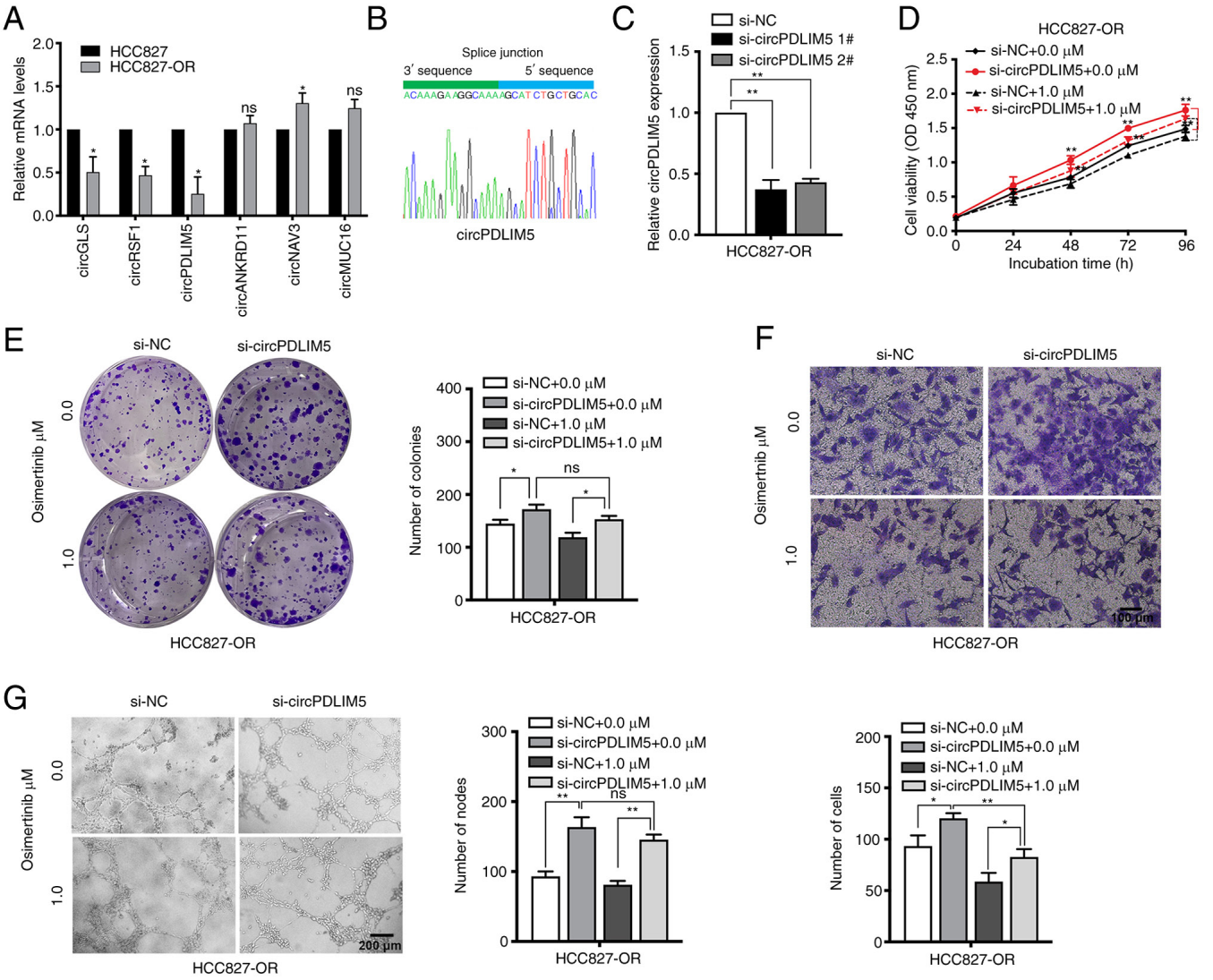

Figure 6. CircPDLIM5 inhibits oncogenic progression of HCC827-OR cells in terms of proliferation, migration and angiogenesis. The presence of circPDLIM5 was (A) validated by reverse transcription-quantitative PCR in HCC827 and HCC827-OR cells, followed by (B) Sanger sequencing. (C) Expression of circPDLIM5 in HCC827-OR cells was inhibited by specific siRNAs. (D) Cell Counting Kit 8 and (E) colony formation assays were used to evaluate the cell proliferation of circPDLIM5-depleted HCC827-OR cells treated with or without osimertinib (1 μM). (F) Detection of changes in cell migration in response to osimertinib in transfected HCC826-OR cells. (G) Measurement of tube formation in human umbilical vein endothelial cells to analyze whether circPDLIM5 has an impact on the use of osimertinib in HCC827-OR cells. *P<0.05 and **P<0.01 vs. HCC827 or as indicated. NC, negative control; ns, not significant; si, small interfering.

Discussion

EGFR is one of the driver genes closely related to the occurrence and development of NSCLC. EGFR-TKIs targeting EGFR have improved the survival of patients with lung cancer, bringing marked efficacy to patients with EGFR mutations. In particular, osimertinib, a third-generation irreversible EGFR-TKI, has achieved significant clinical benefits in both first-line and second-line treatment. Notably, the effect of osimertinib has brought great hope for patients with NSCLC; however, most of the patients still have inevitable disease progression, which is usually caused by the generation of acquired resistance to osimertinib (34). Osimertinib resistance in tumors is caused by the regulation of a multi-factor network, and there is still a lack of clinically applicable efficacy prediction markers and effective intervention strategies based on drug resistance molecular mechanisms. With the occurrence of osimertinib resistance, it is necessary to discover the possible mechanisms of osimertinib resistance in advance and to formulate effective strategies (12).

In a previous study, a gefitinib-resistant PC9 cell line was established by stepwise escalation method: Parental PC9 cells were cultured with a stepwise escalation in gefitinib concentration from 5 nM to 5 μM over 6 months (35). In order to explore the mechanism of osimertinib resistance, the present study established osimertinib-resistant cell lines. The method of establishment in the present study is similar to the clinical low-dose administration method of osimertinib. After 10 months, osimertinib-resistant cell lines HCC827-OR and H1975-OR were successfully induced. Verusingam *et al* (36) previously generated an osimertinib-resistant cell line from H1975, whereas the present study developed two resistant cell lines. Sensitive and resistant cell lines were then treated with different concentrations of osimertinib, and the specific differences between

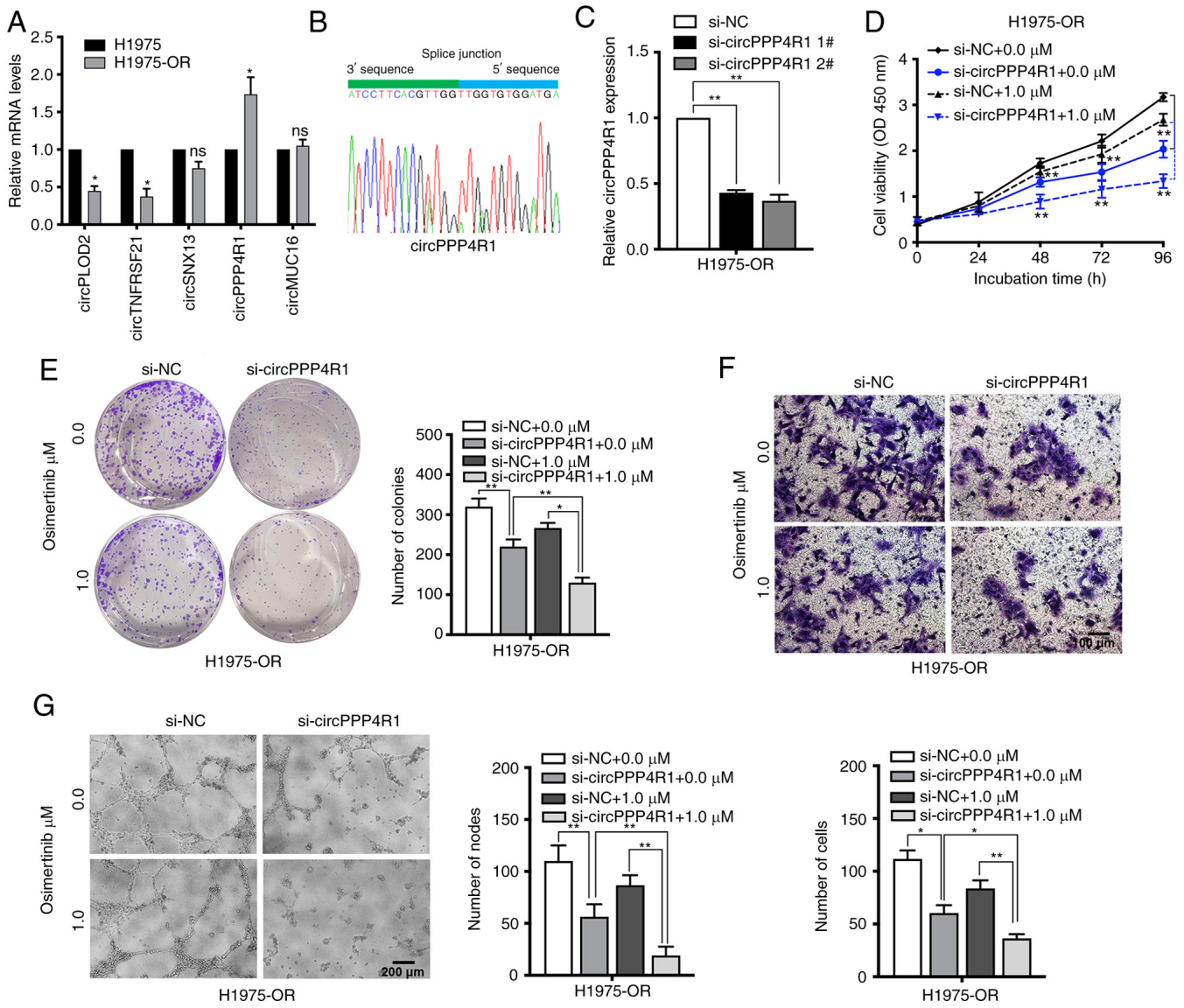

Figure 7. Downregulation of circPPP4R1 increase the sensitivity of H1975-OR cells to osimertinib. The presence of circPPP4R1 was (A) validated by RT-qPCR in H1975 and H1975-OR cells, followed by (B) Sanger sequencing. (C) RT-qPCR analysis of circPPP4R1 expression levels in H1975-OR cells transfected with two discrete chemically synthesized siRNAs. H1975-OR and circPPP4R1-depleted H1975-OR cells treated with or without osimertinib (1 μM) were assessed by (D) Cell Counting Kit 8 assay, (E) colony formation assay, (F) Transwell assay and (G) tube-formation assays. *P<0.05 and **P<0.01 vs. H1975 or as indicated. NC, negative control; ns, not significant; RT-qPCR, reverse transcription-quantitative PCR; si, small interfering.

sensitive and resistant cell lines were analyzed. Tian *et al* (9) established three resistant cell lines, PC9, HCC827 and H1975. Cao *et al* (11) also used osimertinib-resistant cell lines to explore the potential mechanism of osimertinib resistance; however, details of the method of establishment were not provided.

The present study demonstrated that the drug-resistant cells HCC827-OR and H1975-OR had considerably elevated levels of p-AKT and p-ERK compared with in parental cells. In addition, the inhibitory effect of osimertinib on p-AKT and p-ERK was less pronounced in the resistant cells than in the parental cells. By contrast, HCC827-OR cells exhibited a clearer inhibitory impact of osimertinib on p-EGFR. The preliminary findings of Tian *et al* (9) are in agreement with the present study. In PC9 osimertinib-resistant cells, ERK was significantly activated and AKT/GSK3β were partially activated in PC9-osimertinib resistant cells. AKT was the dominant activated signaling factor, not ERK, in HCC827-osimertinib resistant and H1975-osimertinib resistant cells. These findings indicated that ERK and AKT activation may be contributors to osimertinib resistance (9). Booth *et al* (10) also found activated AKT in osimertinib-resistant cells.

circRNAs have been identified as a novel class of non-coding RNA, which are different from traditional linear RNAs. It has become known that circRNAs function in multiple biological processes and are involved in several types of cancer (37-40). circ-0003418 exerts an antitumorigenic role in hepatocellular carcinoma (HCC) and advances the sensitivity of HCC cells to cisplatin by restraining the Wnt/β-catenin pathway (41). circPVT1 is related with the cisplatin and pemetrexed insensitivity of patients with lung adenocarcinoma; notably, circPVT1 contributes to cisplatin and pemetrexed chemotherapy resistance through the miR-145-5p/ABCC1 axis (42). Hsa_circ_0005576 promotes osimertinib resistance through the miR-512-5p/IGF1R axis in lung adenocarcinoma cells (43). Inhibition of circ7312 reduces osimertinib resistance by promoting pyroptosis and

apoptosis through the miR-764/MAPK1 axis (44). METTL3 initiates the m6A modification of circKRT17, thereby enhancing the stability of YAP1 by recruiting EIF4A4 and promoting osimertinib resistance in lung adenocarcinoma (45). Hsa_circRNA_0002130 is upregulated in the serum exosomes of patients with osimertinib-resistant NSCLC and is closely associated with glycolysis (21). These previous findings indicated that circRNA may have a key regulatory role in tumorigenesis and drug resistance. Although there are some reports on circRNA and osimertinib resistance in lung cancer, the complex mechanism underlying circRNA dysregulation and their biological effects has not been clearly elucidated.

The present study screened the differentially expressed circRNAs between HCC827, HCC827-OR, H1975 and H1975-OR cells by high-throughput sequencing. KEGG pathway analysis revealed that the host genes of differentially expressed circRNAs in resistant and sensitive cells were mainly associated with regulation of autophagy. Compared with in the parental cells, HCC827-OR and H1975-OR cells showed reduced protein levels of P62 and an increase in LC3-II conversion, indicating that the resistant cell lines may have increased autophagy levels, which is consistent with previous results (11). Current studies have shown that inhibition of autophagy can increase the sensitivity of tumor cells to drugs, and the activation of autophagy can lead to increased drug resistance in tumor cells (46-48). Osimertinib has also been shown to induce autophagy in NSCLC cell lines (11). Drug-resistant cells have increased autophagy activity when compared with their sensitive parental cells. A novel anticancer drug GZ17-6.02 that interacts with osimertinib can increase autophagosome formation (10). Increased protective autophagy may be one of the mechanisms underlying NSCLC resistance to EGFR-TKIs (11).

The present study validated the RNA-seq results and chose the most dysregulated circRNAs (circPDLIM5 and circPPP4R1) for further study. *In vitro* studies showed that knockdown of circPDLIM5 could promote HCC827-OR cell proliferation, migration and angiogenesis, and inhibit apoptosis. By contrast, inhibition of circPPP4R1 could reduce H1975-OR cell proliferation, migration and angiogenesis, and promote apoptosis. Through the establishment and analysis of drug-resistant cell lines, novel mechanisms and pathways in drug resistance may be identified, which can lay a foundation for further research and provide a scientific basis for clinical drug use.

In conclusion, the present study established osimertinib-resistant cell lines and revealed the aberrant expression of circRNAs. The results indicated that circRNAs may have important roles in NSCLC osimertinib resistance, providing potential diagnostic or therapeutic biomarkers for EGFR-TKI therapy of NSCLC. Further studies should be conducted to further the investigation of the mechanism underlying osimertinib resistance.

Acknowledgements

Not applicable.

Funding

This work was supported by grants from the National Natural Science Foundation of China (grant nos. 82072591 and 82203058), the Key Research and Development Plan (Social Development) of Science And Technology Department of Jiangsu Province (grant no. BE2019760), the Jiangsu Province Capability Improvement Project through Science, Technology and Education, Jiangsu Provincial Medical Key Discipline Cultivation Unit (grant no. JSDW202235), the '789' Excellent Talent Training Plan of the Second Affiliated Hospital of Nanjing Medical University (grant no. 789ZYRC202090146), and the China Postdoctoral Science Foundation (grant nos. 2022M710753 and 2023T160120).

Availability of data and materials

The high-throughput RNA sequencing and NGS data in the present study have been deposited in the BioProject (https://www.ncbi.nlm.nih.gov/bioproject/) under accession number PRJNA1000087 (https://www.ncbi.nlm.nih.gov/bioproject/PRJNA1000087/) and PRJNA1000497 (https://www.ncbi.nlm.nih.gov/bioproject/PRJNA1000497/).The other datasets used and/or analyzed during the current study are available from the corresponding author on reasonable request.

Authors' contributions

ZXW and ZYC designed the study. XC, JYG and JLH designed the main experiments, detected the cell biological function, conducted the RT-qPCR analysis, performed the statistical analysis, and wrote the manuscript. KW and GZ participated in the design of the experiments and statistical analysis. JLH and KW carried out the western blot analyses. All authors read and approved the final manuscript. XC and ZXW confirm the authenticity of all the raw data.

Ethics approval and consent to participate

Not applicable.

Patient consent for publication

Not applicable.

Competing interests

The authors declare that they have no competing interests.

References

1. Sung H, Ferlay J, Siegel RL, Laversanne M, Soerjomataram I, Jemal A and Bray F: Global cancer statistics 2020: GLOBOCAN estimates of incidence and mortality worldwide for 36 cancers in 185 countries. CA Cancer J Clin 71: 209-249, 2021.
2. Testa U, Castelli G and Pelosi E: Lung cancers: Molecular characterization, clonal heterogeneity and evolution, and cancer stem cells. Cancers (Basel) 10: 248, 2018.
3. Normanno N, Maiello MR, Chicchinelli N, Iannaccone A, Esposito C, De Cecio R, D'alessio A and De Luca A: Targeting the EGFR T790M mutation in non-small-cell lung cancer. Expert Opin Ther Targets 21: 159-165, 2017.
4. Ramalingam SS, Vansteenkiste J, Planchard D, Cho BC, Gray JE, Ohe Y, Zhou C, Reungwetwattana T, Cheng Y, Chewaskulyong B, *et al*: Overall survival with osimertinib in untreated, EGFR-mutated advanced NSCLC. N Engl J Med 382: 41-50, 2020.

5. Nagasaka M, Zhu VW, Lim SM, Greco M, Wu F and Ou SI: Beyond osimertinib: the development of third-generation EGFR tyrosine kinase inhibitors for advanced EGFR+ NSCLC. J Thorac Oncol 16: 740-763, 2021.
6. Park S and Ahn MJ: Osimertinib in central nervous system progressive EGFR-mutant lung cancer: Do we need to detect T790M? Ann Oncol 31: 1582, 2020.
7. Nakatani K, Yamaoka T, Ohba M, Fujita KI, Arata S, Kusumoto S, Taki-Takemoto I, Kamei D, Iwai S, Tsurutani J and Ohmori T: KRAS and EGFR amplifications mediate resistance to rociletinib and osimertinib in acquired afatinib-resistant NSCLC harboring exon 19 deletion/T790M in EGFR. Mol Cancer Ther 18: 112-126, 2019.
8. Nishiyama A, Takeuchi S, Adachi Y, Otani S, Tanimoto A, Sasaki M, Matsumoto S, Goto K and Yano S: MET amplification results in heterogeneous responses to osimertinib in EGFR-mutant lung cancer treated with erlotinib. Cancer Sci 111: 3813-3823, 2020.
9. Tian X, Wang R, Gu T, Ma F, Laster KV, Li X, Liu K, Lee MH and Dong Z: Costunolide is a dual inhibitor of MEK1 and AKT1/2 that overcomes osimertinib resistance in lung cancer. Mol Cancer 21: 193, 2022.
10. Booth L, West C, Moore RP, Von Hoff D and Dent P: GZ17-6.02 and pemetrexed interact to kill osimertinib-resistant NSCLC cells that express mutant ERBB1 proteins. Front Oncol 11: 711043, 2021.
11. Cao P, Li Y, Shi R, Yuan Y, Gong H, Zhu G, Zhang Z, Chen C, Zhang H, Liu M, *et al*: Combining EGFR-TKI with SAHA overcomes EGFR-TKI-acquired resistance by reducing the protective autophagy in non-small cell lung cancer. Front Chem 10: 837987, 2022.
12. Fu K, Xie F, Wang F and Fu L: Therapeutic strategies for EGFR-mutated non-small cell lung cancer patients with osimertinib resistance. J Hematol Oncol 15: 173, 2022.
13. Ebbesen KK, Hansen TB and Kjems J: Insights into circular RNA biology. RNA Biol 14: 1035-1045, 2017.
14. Huang W, Yang Y, Wu J, Niu Y, Yao Y, Zhang J, Huang X, Liang S, Chen R, Chen S and Guo L: Circular RNA cESRP1 sensitises small cell lung cancer cells to chemotherapy by sponging miR-93-5p to inhibit TGF-β signalling. Cell Death Differ 27: 1709-1727, 2020.
15. Wang C, Tan S, Li J, Liu WR, Peng Y and Li W: CircRNAs in lung cancer-biogenesis, function and clinical implication. Cancer Lett 492: 106-115, 2020.
16. Wang T, Liu Z, She Y, Deng J, Zhong Y, Zhao M, Li S, Xie D, Sun X, Hu X and Chen C: A novel protein encoded by circASK1 ameliorates gefitinib resistance in lung adenocarcinoma by competitively activating ASK1-dependent apoptosis. Cancer Lett 520: 321-331, 2021.
17. Zhang LX, Gao J, Long X, Zhang PF, Yang X, Zhu SQ, Pei X, Qiu BQ, Chen SW, Lu F, *et al*: The circular RNA circHMGB2 drives immunosuppression and anti-PD-1 resistance in lung adenocarcinomas and squamous cell carcinomas via the miR-181a-5p/CARM1 axis. Mol Cancer 21: 110, 2022.
18. Zhang PF, Pei X, Li KS, Jin LN, Wang F, Wu J and Zhang XM: Circular RNA circFGFR1 promotes progression and anti-PD-1 resistance by sponging miR-381-3p in non-small cell lung cancer cells. Mol Cancer 18: 179, 2019.
19. Wen C, Xu G, He S, Huang Y, Shi J, Wu L and Zhou H: Screening circular RNAs related to acquired gefitinib resistance in non-small cell lung cancer cell lines. J Cancer 11: 3816-3826, 2020.
20. Chen T, Luo J, Gu Y, Huang J, Luo Q and Yang Y: Comprehensive analysis of circular RNA profiling in AZD9291-resistant non-small cell lung cancer cell lines. Thorac Cancer 10: 930-941, 2019.
21. Ma J, Qi G and Li L: A novel serum exosomes-based biomarker hsa_circ_0002130 facilitates osimertinib-resistance in non-small cell lung cancer by sponging miR-498. Onco Targets Ther 13: 5293-5307, 2020.
22. Pan J, Xing J, Yu H, Wang Z, Wang W and Pan Y: CircRBM33 promotes migration, invasion and mediates osimertinib resistance in non-small cell lung cancer cell line. Ann Transl Med 11: 252, 2023.
23. Tang ZH, Jiang XM, Guo X, Fong CM, Chen X and Lu JJ: Characterization of osimertinib (AZD9291)-resistant non-small cell lung cancer NCI-H1975/OSIR cell line. Oncotarget 7: 81598-81610, 2016.
24. Schmittgen TD and Livak KJ: Analyzing real-time PCR data by the comparative C(T) method. Nat Protoc 3: 1101-1108, 2008.
25. Damgaard MV and Treebak JT: Protocol for qPCR analysis that corrects for cDNA amplification efficiency. STAR Protoc 3: 101515, 2022.
26. Koboldt DC, Zhang Q, Larson DE, Shen D, McLellan MD, Lin L, Miller CA, Mardis ER, Ding L and Wilson RK: VarScan 2: Somatic mutation and copy number alteration discovery in cancer by exome sequencing. Genome Res 22: 568-576, 2012.
27. Talevich E, Shain AH, Botton T and Bastian BC: CNVkit: Genome-wide copy number detection and visualization from targeted DNA sequencing. PLoS Comput Biol 12: e1004873, 2016.
28. Zhang X, Maity TK, Ross KE, Qi Y, Cultraro CM, Bahta M, Pitts S, Keswani M, Gao S, Nguyen KDP, *et al*: Alterations in the global proteome and phosphoproteome in third generation EGFR TKI resistance reveal drug targets to circumvent resistance. Cancer Res 81: 3051-3066, 2021.
29. Birgisdottir ÅB and Johansen T: Autophagy and endocytosis-interconnections and interdependencies. J Cell Sci 133: jcs228114, 2020.
30. Ganapathy AS, Saha K, Suchanec E, Singh V, Verma A, Yochum G, Koltun W, Nighot M, Ma T and Nighot P: AP2M1 mediates autophagy-induced CLDN2 (claudin 2) degradation through endocytosis and interaction with LC3 and reduces intestinal epithelial tight junction permeability. Autophagy 18: 2086-2103, 2022.
31. Nnah IC, Wang B, Saqcena C, Weber GF, Bonder EM, Bagley D, De Cegli R, Napolitano G, Medina DL, Ballabio A and Dobrowolski R: TFEB-driven endocytosis coordinates MTORC1 signaling and autophagy. Autophagy 15: 151-164, 2019.
32. Yochum ZA, Cades J, Wang H, Chatterjee S, Simons BW, O'Brien JP, Khetarpal SK, Lemtiri-Chlieh G, Myers KV, Huang EH, *et al*: Targeting the EMT transcription factor TWIST1 overcomes resistance to EGFR inhibitors in EGFR-mutant non-small-cell lung cancer. Oncogene 38: 656-670, 2019.
33. Yu HA, Schoenfeld AJ, Makhnin A, Kim R, Rizvi H, Tsui D, Falcon C, Houck-Loomis B, Meng F, Yang JL, *et al*: Effect of osimertinib and bevacizumab on progression-free survival for patients with metastatic EGFR-mutant lung cancers: A phase 1/2 single-group open-label trial. JAMA Oncol 6: 1048-1054, 2020.
34. Tang ZH and Lu JJ: Osimertinib resistance in non-small cell lung cancer: Mechanisms and therapeutic strategies. Cancer Lett 420: 242-246, 2018.
35. Chen Z, Chen Q, Cheng Z, Gu J, Feng W, Lei T, Huang J, Pu J, Chen X and Wang Z: Long non-coding RNA CASC9 promotes gefitinib resistance in NSCLC by epigenetic repression of DUSP1. Cell Death Dis 11: 858, 2020.
36. Verusingam ND, Chen YC, Lin HF, Liu CY, Lee MC, Lu KH, Cheong SK, Han-Kiat Ong A, Chiou SH and Wang ML: Generation of osimertinib-resistant cells from epidermal growth factor receptor L858R/T790M mutant non-small cell lung carcinoma cell line. J Chin Med Assoc 84: 248-254, 2021.
37. Kristensen LS, Andersen MS, Stagsted LVW, Ebbesen KK, Hansen TB and Kjems J: The biogenesis, biology and characterization of circular RNAs. Nat Rev Genet 20: 675-691, 2019.
38. Kristensen LS, Jakobsen T, Hager H and Kjems J: The emerging roles of circRNAs in cancer and oncology. Nat Rev Clin Oncol 19: 188-206, 2022.
39. Li R, Jiang J, Shi H, Qian H, Zhang X and Xu W: CircRNA: A rising star in gastric cancer. Cell Mol Life Sci 77: 1661-1680, 2020.
40. Zhang M, Bai X, Zeng X, Liu J, Liu F and Zhang Z: circRNA-miRNA-mRNA in breast cancer. Clin Chim Acta 523: 120-130, 2021.
41. Chen H, Liu S, Li M, Huang P and Li X: circ_0003418 inhibits tumorigenesis and cisplatin chemoresistance through Wnt/β-catenin pathway in hepatocellular carcinoma. Onco Targets Ther 12: 9539-9549, 2019.
42. Zheng F and Xu R: CircPVT1 contributes to chemotherapy resistance of lung adenocarcinoma through miR-145-5p/ABCC1 axis. Biomed Pharmacother 124: 109828, 2020.
43. Liu S, Jiang Z, Xiao P, Li X, Chen Y, Tang H, Chai Y, Liu Y, Zhu Z, Xie Q, *et al*: Hsa_circ_0005576 promotes osimertinib resistance through the miR-512-5p/IGF1R axis in lung adenocarcinoma cells. Cancer Sci 113: 79-90, 2022.
44. Dai C, Ma Z, Si J, An G, Zhang W, Li S and Ma Y: Hsa_circ_0007312 promotes third-generation epidermal growth factor receptor-tyrosine kinase inhibitor resistance through pyroptosis and apoptosis via the MiR-764/MAPK1 axis in lung adenocarcinoma cells. J Cancer 13: 2798-2809, 2022.

45. Ji Y, Zhao Q, Feng W, Peng Y, Hu B and Chen Q: N6-methyladenosine modification of CIRCKRT17 initiated by METTL3 promotes osimertinib resistance of lung adenocarcinoma by EIF4A3 to enhance YAP1 stability. Cancers (Basel) 14: 5582, 2022.
46. Lin Z, Niu Y, Wan A, Chen D, Liang H, Chen X, Sun L, Zhan S, Chen L, Cheng C, *et al*: RNA m^6A methylation regulates sorafenib resistance in liver cancer through FOXO3-mediated autophagy. EMBO J 39: e103181, 2020.
47. Luo Y, Zheng S, Wu Q, Wu J, Zhou R, Wang C, Wu Z, Rong X, Huang N, Sun L, *et al*: Long noncoding RNA (lncRNA) EIF3J-DT induces chemoresistance of gastric cancer via autophagy activation. Autophagy 17: 4083-4101, 2021.
48. Paquette M, El-Houjeiri L, C Zirden L, Puustinen P, Blanchette P, Jeong H, Dejgaard K, Siegel PM and Pause A: AMPK-dependent phosphorylation is required for transcriptional activation of TFEB and TFE3. Autophagy 17: 3957-3975, 2021.